Biomaterials Science

PAPER

View Article Online
View Journal | View Issue

Cite this: *Biomater. Sci.*, 2026, **14**, 2416

Exosome–niosome hybrid oxygen carrier for protection against acetaminophen-induced acute liver injury

Anika Bushra, [a,d] Dalton Jayne, [b,d] Thomas Locke, [b,d] Xiaoxue Han, [b,d] Timothy M. Fan, [e,f] Gregory H. Underhill [b] and Joseph Irudayaraj *[b,c,d,f]

Acetaminophen (APAP) overdose is one of the contributing factors for acute liver injury (ALI), caused by a hypoxic microenvironment, elevated oxidative stress, and pro-inflammatory signaling. In this work, we present an exosome–niosome hybrid oxygen carrier (ENh-OC) composed of polysorbate 80, Pluronic® F-127, medium chain triglyceride oil, and blueberry-derived exosomes. We propose that our delivery system shields the liver tissue from localized hypoxia by maintaining sustained oxygen delivery, and the antioxidant and anti-inflammatory components present in the exosomes enhance the hepatoprotective effect. The hydrodynamic diameter of ENh-OCs is 74.0 ± 30.8 nm with a zeta potential of −13.2 ± 0.5 mV, and oxygen holding capacity of 54.3 ± 1.5 mg L^{-1}. They have a shelf life of up to 6 months at 4 °C, and an extended oxygen release profile of up to 16 hours under physiological hypoxic conditions. ENh-OCs have demonstrated excellent mitigative effects against hypoxia, reactive oxygen species, and superoxide-induced damage in LX-2 and HepG2 cell lines under 24 hours of sustained hypoxia. Additionally, ENh-OCs have shown a significant protective effect against APAP-induced cytotoxicity in LX-2spheroids when treated after 24 hours of the initial injury phase. The safety profile of ENh-OCs has been established, and efficacy in protection from APAP-induced ALI has been demonstrated in an *in vivo* murine model. RT-qPCR results verified downregulation of genes related to hypoxia (HIF-1α, VEGF-A), oxidative stress (Nrf2, HO-1), and inflammation (IL-1β, TNF-α) both *in vitro* and *in vivo*. Furthermore, histological analysis revealed protective effects of ENh-OCs against centrilobular necrosis and excessive immune-infiltration. We propose that the novel oxygen nanocarrier platform introduced here might act as a protective agent against APAP-induced ALI.

Received 20th December 2025,
Accepted 25th March 2026

DOI: 10.1039/d5bm01861g

rsc.li/biomaterials-science

Introduction

Acetaminophen, or *N*-acetyl-*p*-aminophenol (APAP), is one of the most prevalent anti-pyretic or analgesic non-prescription drugs worldwide, and a readily accessible over-the-counter medication.[1] The current maximum recommended dose by the U.S. Food and Drug Administration (FDA) is 4000 mg day^{-1} for adults, below which it is generally considered to be safe.[2] Unfortunately, the presence of APAP in numerous prescription and over-the-counter medications is a major reason behind unintentional overdosing, leading to acute liver injury (ALI). In the United States, APAP-overdose results in 60 000–80 000 emergency department visits, half of which lead to hospitalization, with 300–500 annual fatalities.[3] APAP-induced ALI is the leading cause of acute liver failure (ALF) in the United States and much of Western Europe.[4]

APAP-induced ALI begins with initial symptoms such as nausea and vomiting, followed by localized right-upper quadrant abdominal pain, elevated hepatobiliary enzymes, jaundice, coagulopathies, and hepatic encephalopathy in the next four days. Persisting symptoms beyond four days could lead to multi-organ failure and fatality.[1] The mainstay treatment for APAP-induced ALI is intravenous or oral *N*-acetyl cysteine (NAC), which is an antioxidant that regenerates hepatic glutathione content and detoxifies *N*-acetyl-*p*-benzoquinone imine (NAPQI) (a toxic metabolite of APAP).[5] Long-term misuse of APAP has been shown to activate hypoxia-inducible factor-1α (HIF-1α), a transcription factor that controls oxygen homeosta-

[a]*Department of Chemical and Biomolecular Engineering, University of Illinois at Urbana-Champaign, Urbana, Illinois 61801, USA*
[b]*Department of Bioengineering, University of Illinois at Urbana-Champaign, Urbana, Illinois 61801, USA. E-mail: jirudaya@illinois.edu*
[c]*Carle-Illinois College of Medicine, University of Illinois at Urbana-Champaign, Urbana, Illinois 61801, USA*
[d]*Biomedical Research Center in Mills Breast Cancer Institute, Carle Foundation Hospital, Urbana, Illinois 61801, USA*
[e]*Department of Veterinary Clinical Medicine, University of Illinois at Urbana-Champaign, Urbana, Illinois 61801, USA*
[f]*Cancer Center at Illinois (CCIL), University of Illinois at Urbana-Champaign, Urbana, Illinois 61801, USA*

sis in response to hypoxia, inflammation, and oxidative stress.[6] Hypoxia mitigation has been investigated as a potential treatment for APAP-induced hepatotoxicity,[7] liver fibrosis,[8] and hepatocellular carcinoma (HCC).[9] One strategy of hypoxia mitigation is hyperbaric oxygen therapy (HBOT), which has shown promise in alleviating early APAP-induced ALI.[10] Additionally, a combination of NAC and HBOT has demonstrated hepatoprotective activity against APAP-induced ALI in a murine model.[11]

A novel and efficacious approach to mitigate hypoxia can involve oxygen delivery nanocarriers, which have been extensively explored by our group.[12–17] Several nano-oxygen carriers have been formulated for combating hypoxic liver pathologies, such as an oxygen-generating catalase-based nanoplatform for liver fibrosis,[18] and Prussian blue oxygen-evolving nanozymes targeting HCC.[19] A promising strategy proposed to improve the bioactivity and bioavailability of oxygen nanocarriers is the incorporation of exosomes, which has been demonstrated in our recent works.[20–22] This current work proposes a novel oxygen delivery nanoplatform that combines the anti-inflammatory and antioxidant properties of exosomes with hypoxia remediation to combat APAP-induced ALI.

Niosomes are spherical bilayered nanovesicles formed from the self-assembly of non-ionic surfactants, where the amphiphilic nature allows for encapsulation of both hydrophobic and hydrophilic drugs.[23] They have several clear advantages over contemporary lipid and polymeric nanoparticles, in terms of safety, inexpensive synthesis and scale-up, along with ease of handling and storage. Exosomes are extracellular vesicles secreted from cells and contain lipids, proteins, nucleic acids, and metabolites, among others, contributing to their therapeutic potential.[24] In recent years, plant-derived exosomes have emerged as a novel class of therapeutics due to reduced immunogenicity compared with animal-sourced exosomes, fewer obstacles in the regulatory pathway, and an abundance and a variety of available raw materials.[25] In this work, we have developed an exosome–niosome hybrid oxygen carrier (ENh-OC), which integrates the therapeutic properties of blueberry-derived exosomes with niosomes for enhanced stability. Blueberry exosomes have shown potential for treating liver pathologies due to their innate ability to mitigate hepatic lipid accumulation, oxidative stress, and inflammatory responses.[26] They have demonstrated efficacy against nonalcoholic fatty liver disease by attenuating oxidative stress, reducing reactive oxygen species (ROS), and preventing cell apoptosis.[27] In this work, we leveraged the anti-inflammatory and antioxidant properties of blueberry exosomes to protect the liver from long-term injuries inflicted due to APAP overdose. Additionally, the proposed ENh-OC supplies oxygen for an extended period, thereby mitigating hepatic hypoxia and protecting the liver tissue from hypoxic cell damage. The proposed hybrid oxygen delivery platform is composed of non-ionic surfactants Pluronic® F-127, polysorbate 80, and medium-chain triglyceride (MCT) oil containing caprylic/capric triglycerides. Pluronic® F-127 and polysorbate 80 are both FDA-approved excipients,[28] while MCTs have an FDA "Generally Recognized as Safe" (GRAS) status,[29] making this oxygen nanocarrier suitable for clinical translation. We propose that the conceived proof-of-concept exosome–niosome hybrid oxygen delivery platform has hepatoprotective effects that could be utilized to combat APAP-induced ALI by targeting hypoxia, oxidative stress, and inflammation.

Results and discussion

Physicochemical characteristics of optimized formulation

The exosome–niosome hybrid oxygen carriers (ENh-OCs) were fabricated by fusing niosome oxygen carriers (N-OCs) with blueberry-derived exosomes (E) using ultrasonic membrane fusion. The schematic of ENh-OC synthesis is depicted in Fig. 1A. With a full factorial design of experiments (DoE), the optimal sonication parameters had an amplitude of 40%, pulse mode, and on–off cycles of 40–30 seconds duration (SI Fig. 1A and B).

Optimal composition was found to be 1×10^{-4} w/v% polysorbate 80, 1×10^{-4} w/v% Pluronic® F-127, 1×10^{-5} w/v% MCT oil, and 0.1 w/v% exosomes (SI Fig. 1C). Standardized effects of each component were calculated using the OriginPro® DoE application (OriginLab Corporation, USA), where exosome concentration was found to have the most significant effect on the size and zeta potential of ENh-OCs (SI Fig. 1D). Additionally, the size of the particles decreased with increasing amplitude, while zeta potential did not have any significant variation (SI Fig. 1E). The effect of the on–off cycle duration was more complex; the size initially increased with the cycle duration, while dipping down for the highest duration of 40–30 seconds. Zeta potential, on the other hand, followed an overall upward trend with cycle duration, except for the 10–5 seconds cycle (SI Fig. 1F).

For the exosomes, the hydrodynamic diameter was 139.3 ± 50.3 nm (Fig. 1B), polydispersity index of 20.6%, and a zeta potential of −23.0 ± 1.1 mV. The hydrodynamic diameters of optimized ENh-OCs were 74.0 ± 30.8 nm (Fig. 1B), a polydispersity index of 24.1%, and a zeta potential of −13.2 ± 0.5 mV. The concentrations of exosomes and ENh-OCs were measured by NTA to be $5.85 \times 10^9 \pm 1.08 \times 10^8$ particles per mL and $3.77 \times 10^9 \pm 6.46 \times 10^7$ particles per mL, respectively (Fig. 1C and D). TEM images revealed the exosomes to have a variety of near spherical shapes with a high deviation in particle size (Fig. 1E) and ENh-OCs to have spherical bilayers (Fig. 1F).

The blueberry-derived exosomes were found to be enriched with antioxidant and anti-inflammatory components from GC-MS analysis (Fig. 2A). Two of the most abundant were 5-hydroxymethyl furfural (~20%)[30] and campesterol (~5%),[31] both of which show antioxidant and anti-inflammatory properties. Other components with similar properties found in smaller quantities were 4-vinylguaiacol[32] and γ-tocopherol.[33] Additionally, antioxidants such as furaneol[34] and 1,2-cyclopentanedione[35] were also present and could play a role in ROS and superoxide scavenging by the ENh-OCs. The exosomes also contained single-stranded DNA (ssDNA) (90.71 ± 1.19 ng

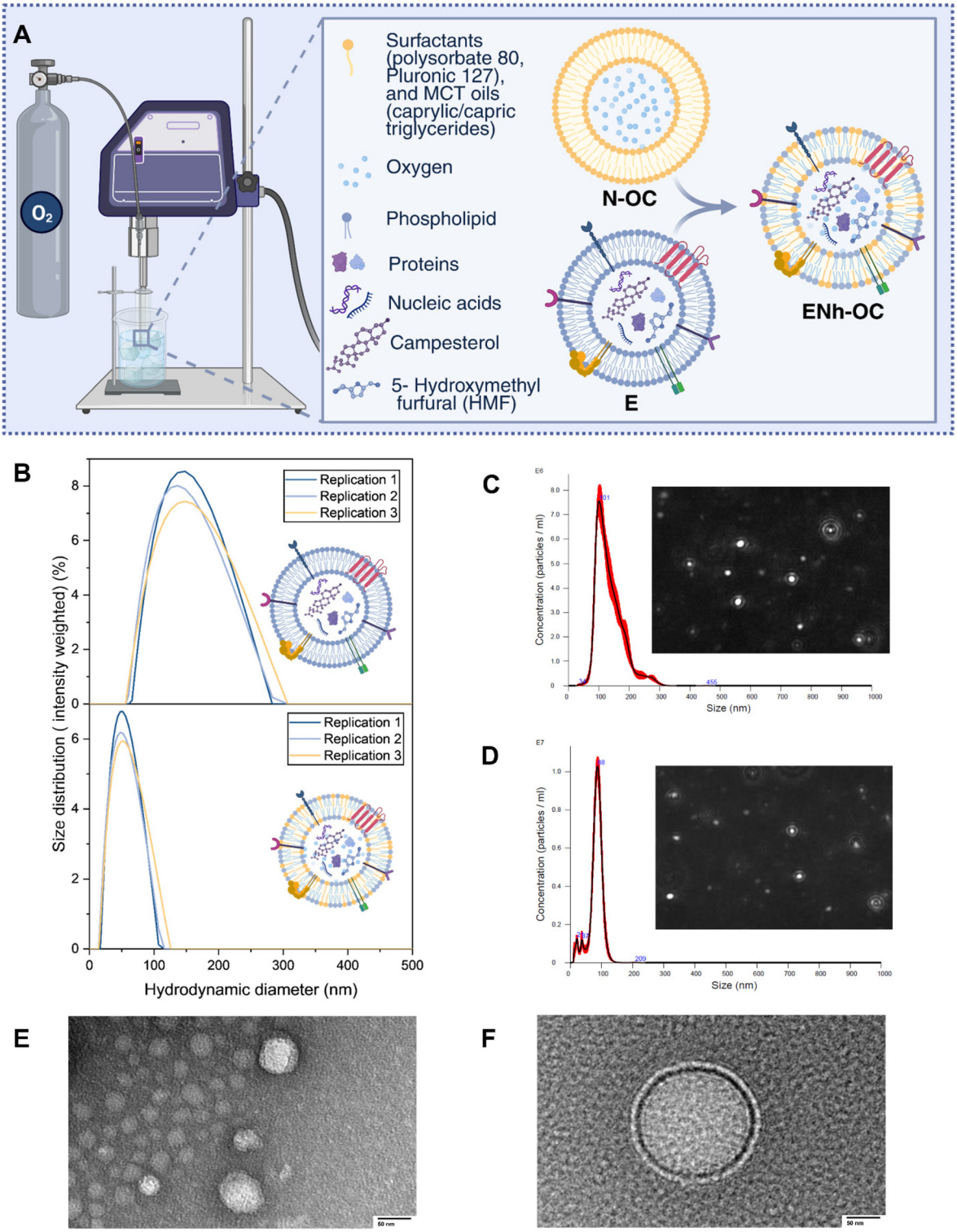

Fig. 1 (A) Exosome–niosome hybrid oxygen carrier (ENh-OC) synthesis by ultrasonication with continued oxygenation, (B) DLS size distribution for blueberry-derived exosomes (top panel), and ENh-OC (bottom panel), particle concentration for exosomes (C), and ENh-OC (D) (inserts show image captured by NTA system), TEM images for exosomes (E), and ENh-OC (F) (scale bar = 50 nm) (Created in https://BioRender.com.).

μL^{-1}), double-stranded DNA (dsDNA) (136.61 ± 0.12 ng μL^{-1}), RNA (109.08 ± 0.11 ng μL^{-1}), and proteins (A280) (2.60 ± 0.02 mg mL^{-1}), as detected *via* UV-Vis spectrophotometer. The combined effect of all these therapeutic molecules present in exosomes could be the key driver behind the inhibition of pro-inflammatory signaling and oxidative stress by ENh-OCs.

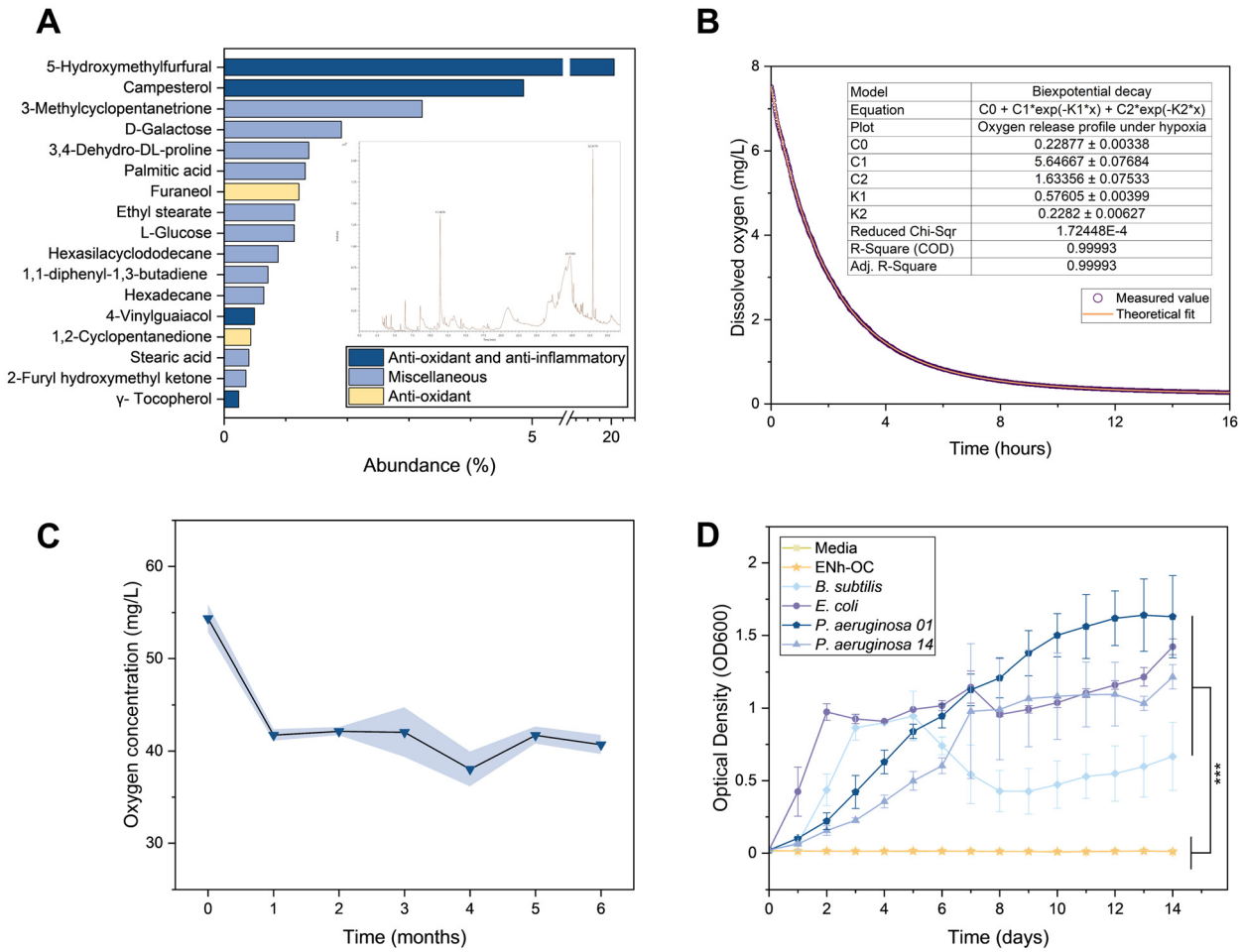

Fig. 2 (A) GC-MS component analysis for blueberry exosomes, with chromatograph in the insert, (B) oxygen release profile under physiological hypoxic conditions (~37 °C, ~0.1% O_2), (C) oxygen retention data for up to 6 months (n = 2), (D) sterility evaluation following US Pharmacopeia Sterility Tests ⟨71⟩ up to 14 days (n = 3).

While different components of blueberry-derived extracellular vesicles are hypothesized to contribute to the therapeutic performance of the ENh-OCs, these effects are not attributed to any specific endogenous marker proteins or lipids, as individual effects of these components have not been explored in this study.

Oxygen release profile, storage stability, and sterility

Oxygen release profiles for ENh-OCs were measured in artificial physiological hypoxic conditions generated in a hypoxia chamber with continued N_2 purging (37 °C, ~0.1% O_2) following previously reported protocol[22] (Fig. 2B). The measured values of DO (dissolved oxygen) over 16 hours were fitted into a biexponential decay kinetic model to quantify oxygen release rate. This biexponential model signifies that there are two regimes of oxygen release, one initial burst release, followed by a slow, controlled release step. The model equation used to fit the experimental data was $C(t) = C_0 + C_1e^{-K_1t} + C_2e^{-K_2t}$ where $C(t)$ is a time-dependent function for dissolved oxygen level in mg L^{-1}, C_0 is residual oxygen at equilibrium in mg L^{-1}, C_1 and C_2 are amplitudes of fast and slow decay functions in mg L^{-1}, respectively, K_1 and K_2 are rate constants for the fast and slow decays, respectively. C_0 was measured as 0.23 mg L^{-1}, meaning this is the residual oxygen after 16 hours, when the ENh-OCs are in equilibrium with the surroundings. C_1 and C_2 were respectively 5.65 mg L^{-1} and 1.63 mg L^{-1}, indicating that oxygen release follows a fast decay between 5.65 and 1.63 mg L^{-1}, and a slow release when the oxygen level falls below 1.63 mg L^{-1}. K_1 and K_2 were 0.58 h^{-1} and 0.23 h^{-1}, respectively. This signifies that, for the fast-release portion, oxygen release rate is 0.58 mg L^{-1} per hour, and this is reduced to 0.23 mg L^{-1} per hour during the slow-release step. This dual oxygen release mechanism holds promise in initial hypoxia relief with a burst release of oxygen, followed by continued oxygen supply. This unique oxygen release profile makes the ENh-OCs especially qualified for prolonged hypoxia mitigation.

The maximum dissolved oxygen concentration in a closed system was recorded as the oxygen loading capacity. The oxygen loading for freshly prepared ENh-OCs was found to be 54.35 ± 1.5 mg L^{-1}, which reduced to 41.73 ± 0.6 mg L^{-1} after

1 month of storage at 4 °C (Fig. 2C). After this initial drop in oxygen content, the level stabilized. The retained oxygen was measured every 4 weeks, and it was found that there was no significant reduction in oxygen during the 6-month study period. This half a year or more of shelf-life stability of the ENh-OCs makes them a compelling candidate for clinical translation. Additionally, sterility evaluation was performed following US Pharmacopeia Sterility Tests ⟨71⟩[36] (Fig. 2D). The positive control samples containing either one of *B. subtilis*, *E. coli*, *P. aeruginosa 01*, or *P. aeruginosa 14* started to show visible bacterial growth from the next day after inoculation, whereas the ENh-OC solution did not show any change in OD600 for up to 14 days. This study confirms that sterility standards were maintained during the synthesis, making this formulation viable for pre-clinical or clinical testing.

Mitigation of hypoxia-induced cell damage, ROS, and superoxide generation

The protective effect of ENh-OCs against cell damage caused by 24-hour sustained hypoxia was evaluated in LX-2 (Fig. 3A) and HepG2 (Fig. 3B) cell lines. In both cell lines, the no-treatment (NT) hypoxia had lowered viability in comparison with NT normoxia. However, with ENh-OC treatment, the cells were protected from hypoxic insult, and the viability was comparable to the normoxic condition. This shows that ENh-OC is capable of preventing hypoxia-induced cellular death, even at a low concentration of 5 v/v%.

Generation of ROS and superoxide is a common occurrence observed under prolonged hypoxia. The inhibitive effect of exosomes (E), ENh-OC shell (ENh-S), and ENh-OC was tested against ROS (Fig. 3C) and superoxide (Fig. 3D) generation under hypoxic conditions. All three treatment groups demonstrated a significant reduction in ROS and superoxide in comparison with the NT groups. This could be attributed to the fact that blueberry exosomes contain natural antioxidant ingredients such as 5-hydroxymethyl furfural, campesterol, 4-vinylguaiacol, γ-tocopherol, furaneol, and 1,2-cyclopentanedione, *etc*. This substantiates ENh-OCs as a potential ROS and superoxide scavenging agent that could help protect from drug-induced hepatic damage.

Enhanced cell uptake

The fusion of E and N-OC was assessed by visualizing the spatial localization of ENh-OCs, where E was labeled with DiO and N-OCs with DiD prior to ENh-OC hybrid formation (Fig. 4A). Fluorescent microscopy revealed a strong spatial co-localization of DiO and DiD signals within the same intracellular compartments, indicating that both membrane components are delivered together as a single entity rather than being internalized independently. While co-localization does

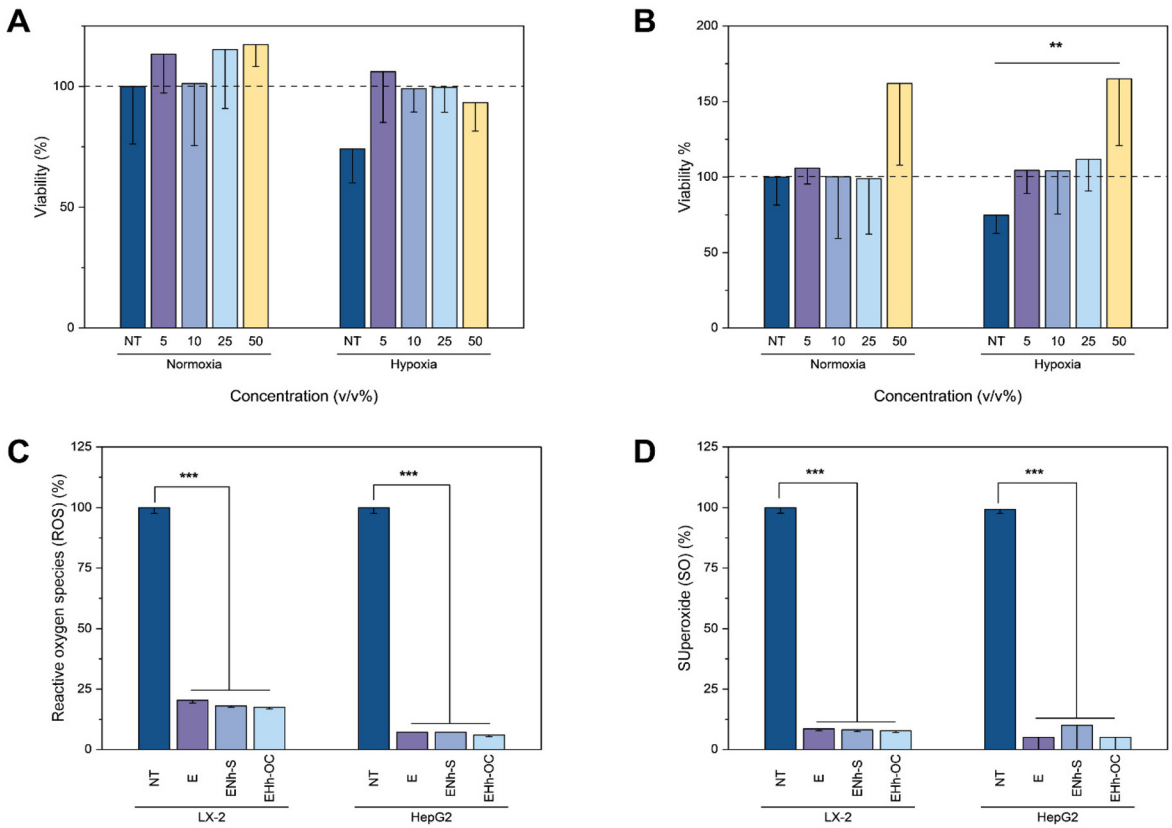

Fig. 3 Evaluation of dose-dependent protective effect of ENh-OC against hypoxia in LX-2 (A) and HepG2 (B) cell lines (n = 8), reactive oxygen species scavenging (C) (n = 4), and superoxide inhibition (D) (n = 4). All cells were incubated under hypoxia for 24 hours.

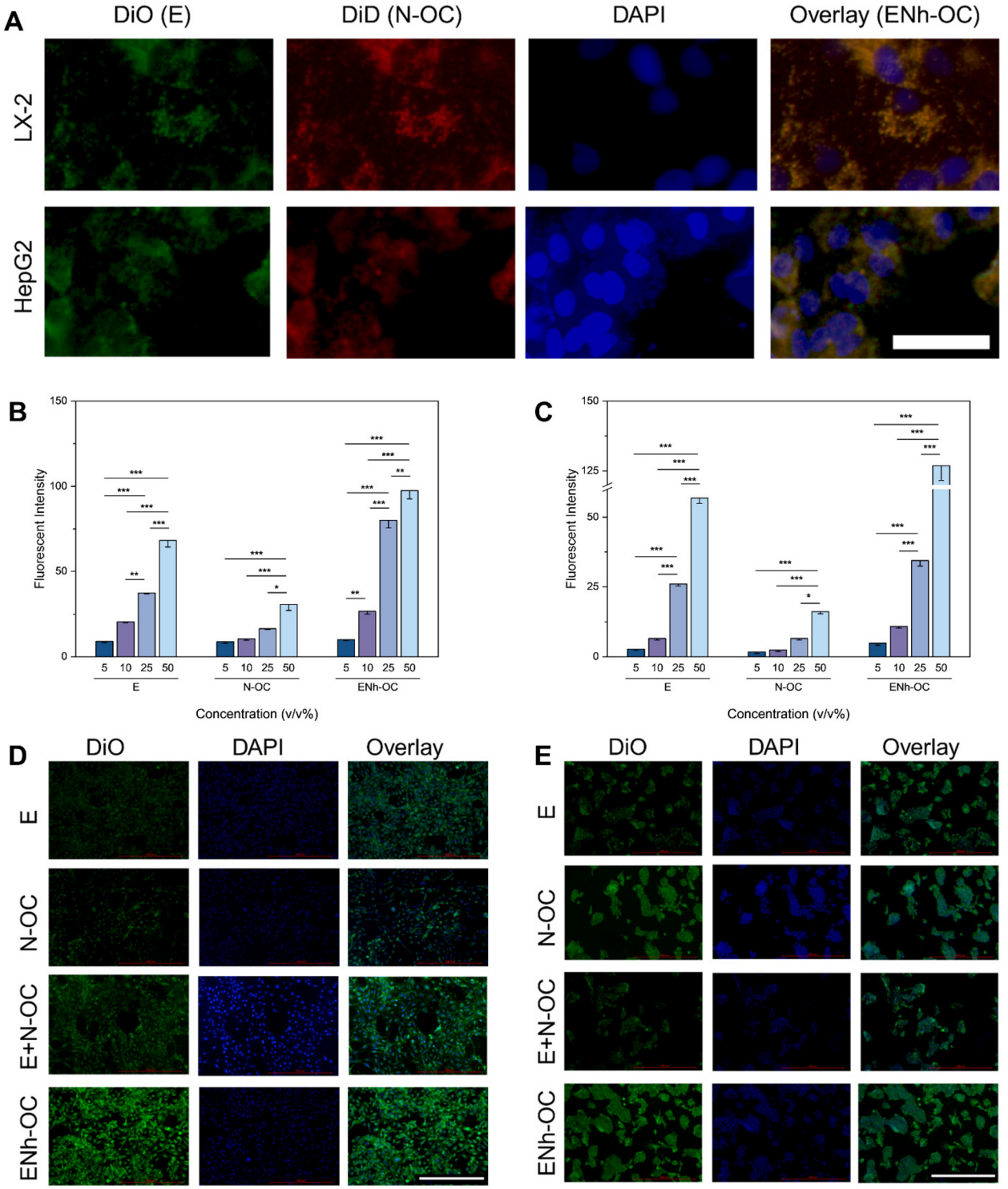

Fig. 4 (A) Evaluation of E and N-OC fusion in LX-2 and HepG2 cell lines (scale bar = 50 μm). Evaluation of dose-dependent cell uptake in LX-2 (B) and HepG2 (C) cell lines with DiO-labeled particles (n = 8). Visualization of uptake in LX-2 (D) and HepG2 (E) with fluorescent imaging (scale bar = 500 μm). *$p \leq 0.05$, **$p \leq 0.01$, and ***$p \leq 0.001$.

not provide direct evidence of lipid mixing at the molecular level, it does demonstrate stable association and joint cellular trafficking of the two membrane components, which is consistent with hybrid carrier formation. Dose-dependent cellular uptake of E, N-OC, and ENh-OC was investigated in LX-2 (Fig. 4B) and HepG2 (Fig. 4C) monolayers. In both cell lines, the ENh-OC particles showed significantly greater uptake than the N-OC groups at the same dose. This might be attributed to

the incorporation of exosomes into the N-OC, which improves uptake *via* potential receptor-mediated endocytosis. Additionally, exosome incorporation might improve cell uptake by facilitating fusion with the cell membrane. This observation is also validated by fluorescent images of LX-2 (Fig. 4D) and HepG2 (Fig. 4E) cells with the endocytosed particles. For this study, one additional group consisting of a physical mixture of E and N-OCs (E + N-OC) was added as a control to show the difference in uptake behaviour between the hybrid and the mixture of E and N-OCs. The uptake of ENh-OC group is considerably higher than E, N-OC, and E + N-OC groups, indicating that this enhanced uptake might be due to the synergistic effect of both oxygen delivery and fusogenic components of exosomes. Additionally, reduced intracellular co-localization and overall uptake of E + N-OCs compared with ENh-OCs demonstrate that simple co-administration of E and N-OC is insufficient to replicate the cellular uptake behaviour of the hybrid carrier, supporting the necessity of the hybrid formulation for enhanced uptake and stable co-delivery.

Modulation of hypoxic, oxidative stress, and inflammatory signaling

The efficacy of ENh-OC in mitigating hypoxia, oxidative stress, and inflammatory signaling was investigated in LX-2 and HepG2 monolayer cultures under 24 hours of prolonged hypoxia. HIF-1α is at the center of hypoxia signaling, and VEGF-A (Vascular Endothelial Growth Factor-A) is one of the key genes modulated by HIF-1α.[37] For gene expression fold change analysis, it was revealed that both HIF-1α (Fig. 5A) and VEGF-A (Fig. 5B) were significantly upregulated under hypoxia (NT(hyp)), in comparison with normoxia (NT(nor)). The treatment groups E, ENh-S, and ENh-OC were able to regulate the expression of HIF-1α and VEGF-A under hypoxia; especially E and ENh-OC were able to keep the expression level near the normoxic levels. This might be attributed to the presence of antioxidant and anti-inflammatory components in the exosomes and oxygen in the ENh-OC in addition to the therapeutic molecules.

The effect of ENh-OC treatment on a couple of antioxidant genes, Nrf2 (Nuclear factor erythroid 2-related factor 2) (Fig. 5C), and HO-1 (Heme Oxygenase-1) (Fig. 5D), was also investigated. Nrf2 is a key biomarker for oxidative stress and is inherently intertwined with HIF-1α signaling. HO-1, on the other hand, is a downstream target gene of both HIF-1α and Nrf2.[38] Both these genes were found to be upregulated under hypoxia, and expression levels with treatments (E, ENh-S, and ENh-OC) were similar to the levels in normoxic conditions. The best results were observed for the ENh-OC treatment group, validating the hypothesis that both oxygen and therapeutic components of blueberry exosomes contribute to this antioxidant effect. Hypoxia and oxidative stress are both closely related to pro-inflammatory signaling.[39] The role of ENh-OC treatment on two pro-inflammatory genes, IL-1β (Interleukin-1 beta) (Fig. 5E), and TNF-α (Tumor Necrosis Factor-alpha) (Fig. 5F), was also explored in this work. Both key players in inflammatory signaling were upregulated under hypoxia. ENh-OC showed the highest anti-inflammatory effect, with exosomes themselves in second place. Even the ENh-S showed considerable anti-inflammatory effect, which might be ascribed to the presence of 5-hydroxymethyl furfural, campesterol, 4-vinylguaiacol, γ-tocopherol, *etc*., present in the exosomes.

Protection against APAP-induced cytotoxicity and uptake in spheroids

The protective effect of ENh-OC against APAP-induced cell damage and toxicity was investigated in the LX-2 spheroid model (Fig. 6A). In this model, APAP was administered on day 1 to induce injury in LX-2 spheroids, followed by ENh-OC treatment on day 2, after injury establishment. Under these conditions, ENh-OC treatment significantly improved cell viability compared to controls, indicating that the formulation can demonstrate a protective effect against APAP injury even when administered after the injury phase. ENh-OC was capable of preventing cell damage and corresponding loss of viability in the spheroids, and the viability of the ENh-OC group was found to be more than that of the no treatment (NT) group (Fig. 6B). This indicates that ENh-OCs not only prevented the cytotoxicity caused by APAP but also contributed to additional cell proliferation due to continued oxygen supply. The E and ENh-S treatment groups also showed some protective effect, as the viability of this group was higher than that of the APAP-only group. The protective effect of ENh-OCs against APAP was also demonstrated by comparing the spheroid sizes on day 3 after APAP treatment, where the spheroids in the APAP group were significantly smaller compared with the NT group. The treatments were found to assist cellular restoration from the APAP damage, with the ENh-OC group having sizes comparable with the NT group (Fig. 6C). The spheroid model has been used as a complementary system alongside the *in vivo* co-administration study to show the effectiveness of ENh-OCs when administered after the initial injury caused by APAP, as evidence of recovery from APAP-induced tissue damage. A major limitation of this current spheroid model is the use of hepatic stellate cells instead of primary hepatocytes to demonstrate the efficacy of ENh-OCs. Further studies with primary hepatocytes are necessary to ascertain the effects of ENh-OCs on the injury phase *versus* the recovery phase, and the translational relevance of this current model. Additionally, cell uptake among E, N-OC, and ENh-OC groups was compared in LX-2/HepG2 spheroids (Fig. 6D). This uptake study in the spheroid model reaffirmed the finding of the 2D monolayer uptake that ENh-OC has considerably more uptake than N-OC (Fig. 6D). This provides evidence that the fusion of exosome membrane components with the niosome shell resulted in enhanced uptake and bioavailability.

In vivo safety and biodistribution evaluation

A safety study was conducted to ascertain the suitability of ENh-OCs in mice. Ten mice were divided into two random groups. One group received ENh-OC tail vein injection (4 doses

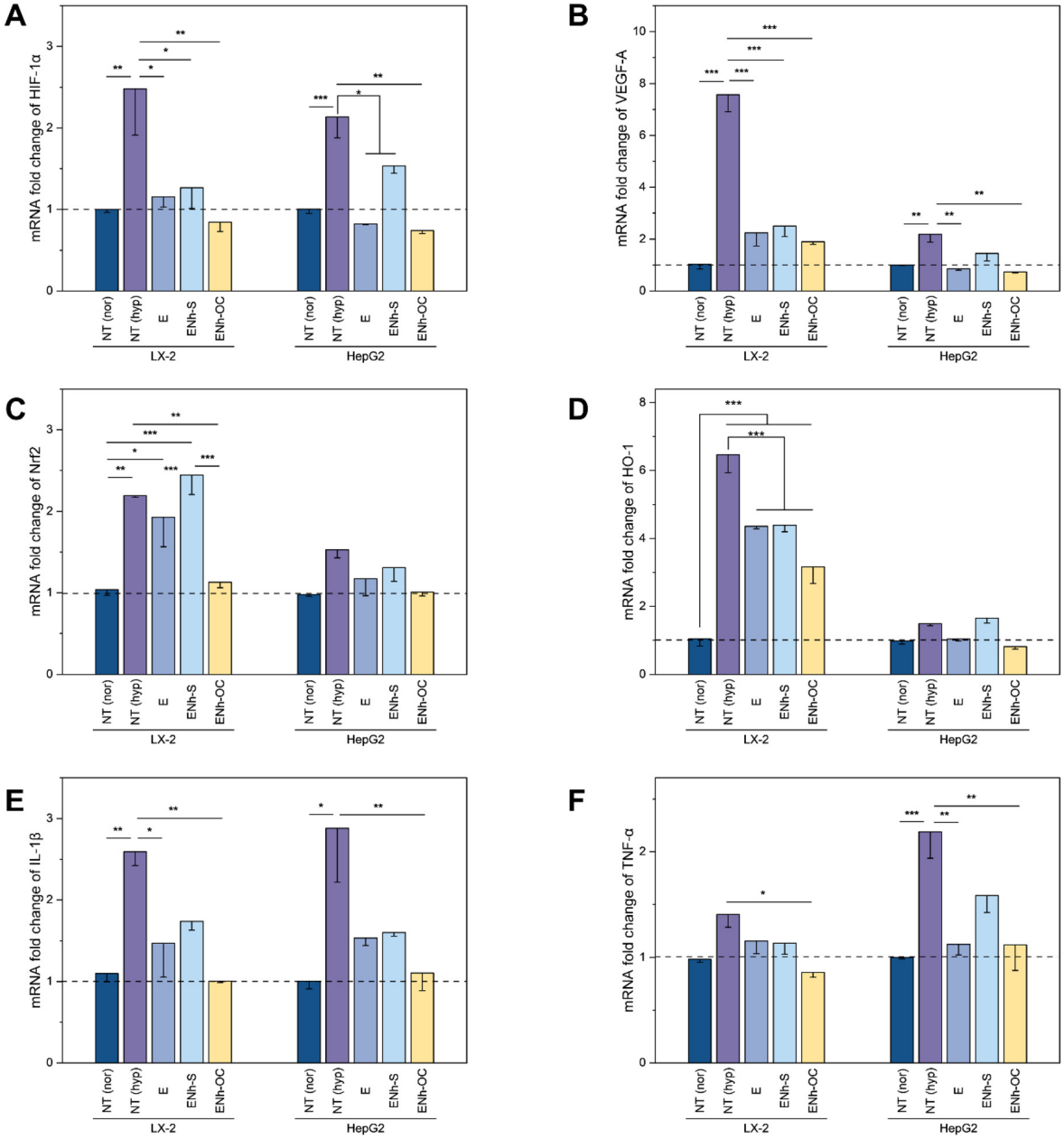

Fig. 5 Modulation of HIF-1α (A), VEGF-A (B), Nrf2 (C), HO-1 (D), IL-1β (E), and TNF-α (F) in LX-2 and HepG2 cell lines. All groups other than NT (nor) were incubated under hypoxia for 24 hours. $n = 3$, $^{*}p \leq 0.05$, $^{**}p \leq 0.01$, and $^{***}p \leq 0.001$.

within a 14-day study period) (Fig. 7A), while the other group received no treatment (NT) and served as a control. H&E stain of the liver, kidney, and lung samples revealed no significant variation between the NT and ENh-OC groups (Fig. 7B). No tissue abnormalities, such as necrosis or upregulated immune infiltration, were observed. This study successfully validated the intravenous administration suitability of ENh-OC, as no systemic toxicity was observed within the two-week timeframe.

An *in vivo* biodistribution study was performed by tail vein administration of DiD-labeled optimized ENh-OCs and monitoring organ distribution with the PerkinElmer IVIS system. Live mice were scanned at 0, 2, 6, 24, 48, 72, and 96-hour intervals post ENh-OC administration, where considerable liver accumulation was observed throughout the study period (Fig. 7C). Additionally, *ex vivo* organs-specific fluorescent distribution after 96 hours showed about 30% of the particles were accumulated in the liver (Fig. 7D). This substantiates the claim that ENh-OCs might be suitable for prolonged oxygen delivery to hypoxic liver tissue.

In vivo efficacy assessment

To assess the efficacy of ENh-OC as a protective agent against APAP-induced ALI, a 3-week study was performed (Fig. 8A). 15 mice were divided into three groups of 5. The groups were

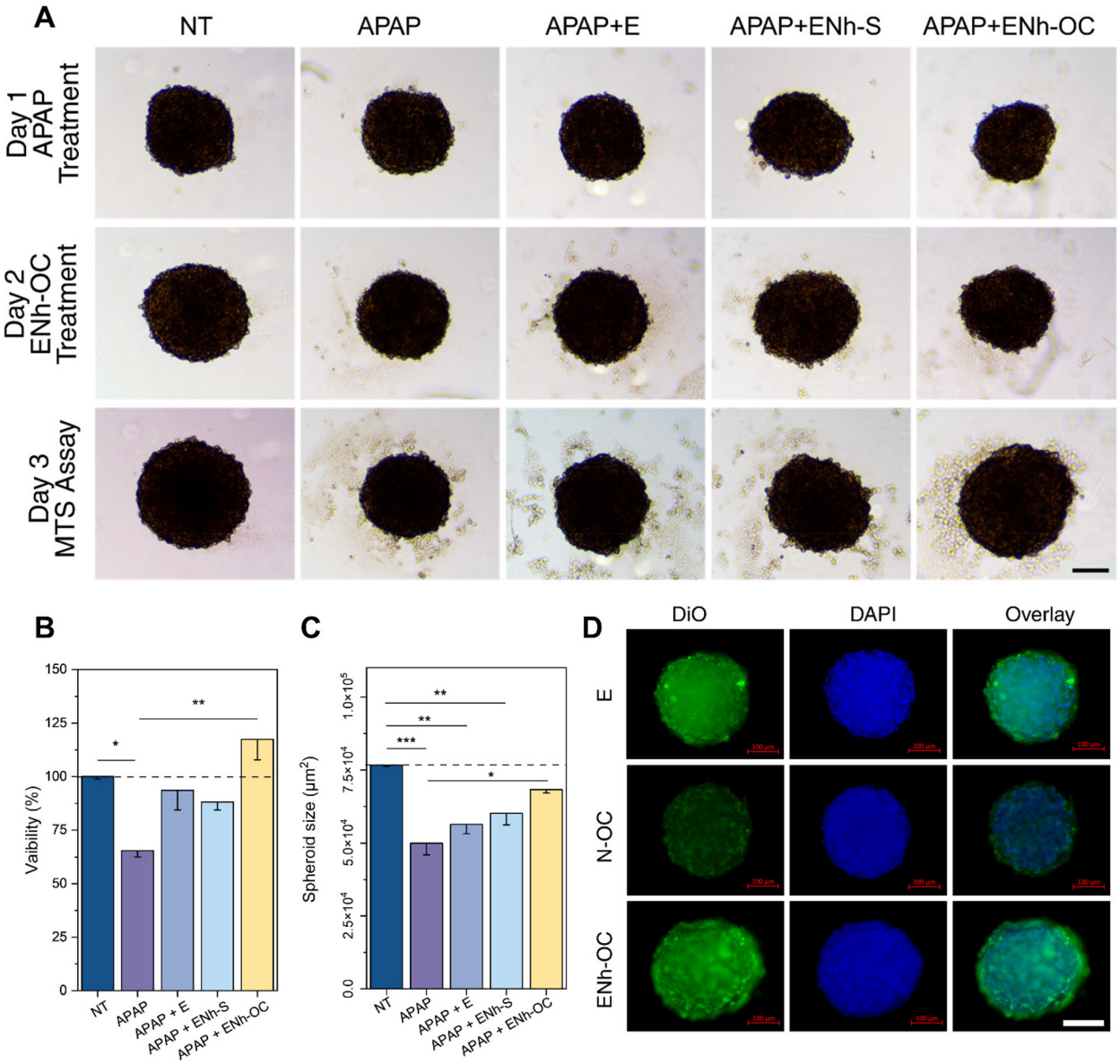

Fig. 6 (A) Evaluation of protection against APAP-induced cytotoxicity in LX-2 spheroids (scale bar = 100 μm), (B) MTS assay to qualify viability of spheroids treated with APAP with different treatment groups, n = 4, (C) spheroid size comparison for spheroids treated with APAP with different treatment groups, n = 4, (D) uptake for DiO-labeled particles in LX-2/HepG2 spheroids (scale bar = 100 μm). *$p \leq 0.05$, **$p \leq 0.01$, and ***$p \leq 0.001$.

no treatment (NT), APAP, and APAP + ENh-OC. H&E-stained liver tissue from the APAP group showed considerable centrilobular necrosis and elevated immune-infiltration (indicated with arrows), indicating activated inflammatory signaling (Fig. 8B). Additionally, the kidney sample of the APAP group showed red blood cells extravasating into the interstitium, and amidst the spaces between the tubules (indicated by arrows) (Fig. 8B). Moreover, the spleen showed increased congestion characterized by excessive distension of sinuses within the red pulp by erythrocytes and elevated white pulp, indicating inflammation (indicated by arrows) (Fig. 8B). The mice that received ENh-OC treatment alongside APAP showed no significant difference from the NT group, indicating that ENh-OC was able to safeguard the liver from APAP toxicity when co-administered. This hypothesis was verified by the TUNEL assay, where the APAP group showed about 3 times more DNA damage than both NT and APAP + ENh-OC groups (Fig. 8C and E). Additionally, IL-1β staining revealed that the liver of APAP-treated mice had about four times more IL-1β than the NT group, whereas the ENh-OC treatment was able to modulate APAP-induced upregulation of cytokine IL-1β, indicating a protective effect (Fig. 8D and F).

The gene expression of hypoxia (HIF-1α, VEGF-A), oxidative stress (Nrf2, HO-1), and inflammation-related (IL-1β, TNF-α) genes in the liver tissues was tested to verify the efficacy of ENh-OC at the genetic level. It was found that all these genes

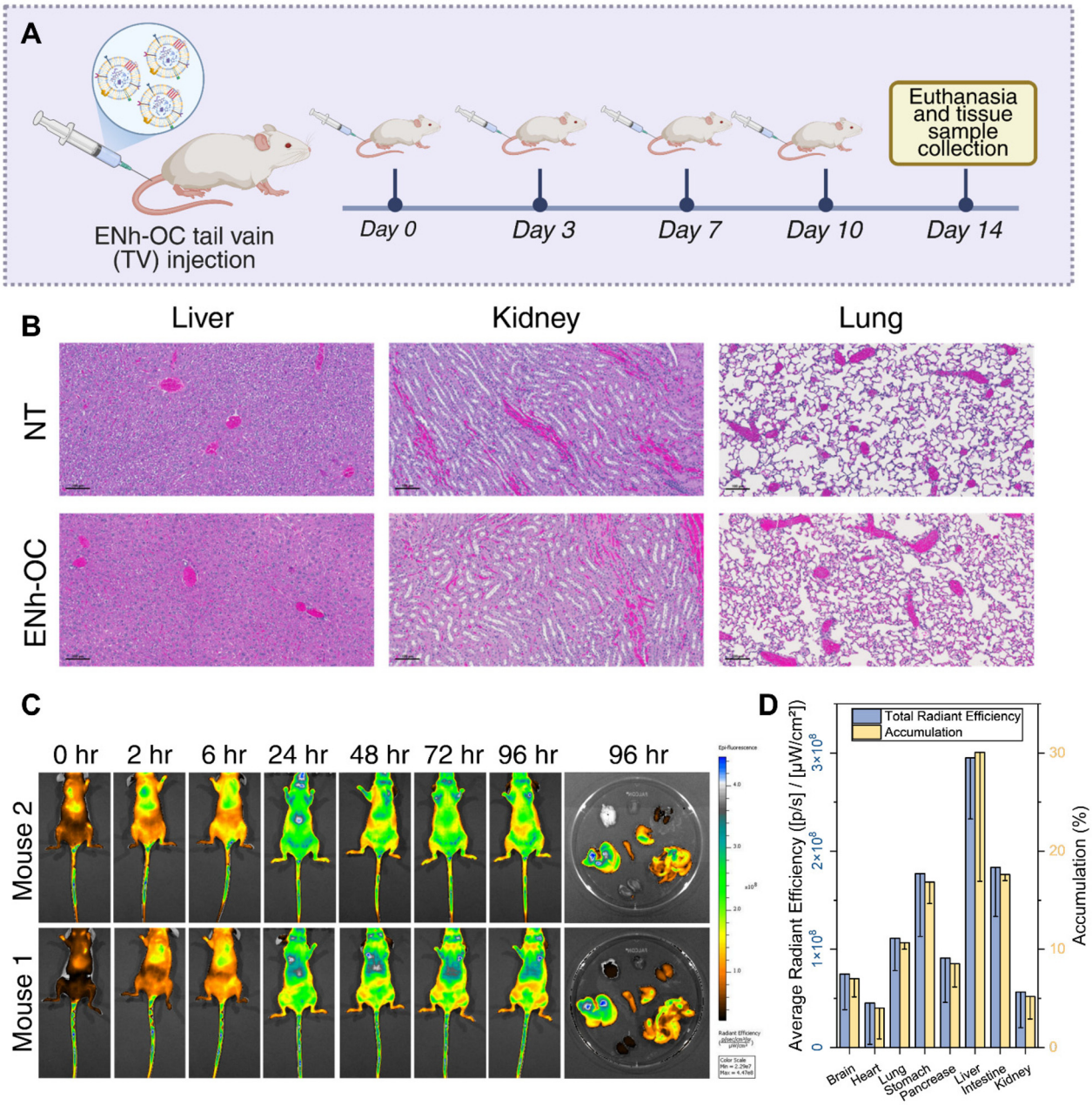

Fig. 7 (A) Timeline for 14-day safety study for ENh-OC intravenous administration (Created in https://BioRender.com.), (B) H&E-stained liver, kidney, and lung samples (scale bar = 100 μm), (C) *in vivo* biodistribution imaging in live mice up to 96 hours, and (D) bar plot depicting average radiant efficiency and percentage accumulation per organ after 96 hours of DiD-labeled ENh-OC tail vein administration (n = 2).

were significantly elevated with APAP administration, but the expression levels were comparable to the NT group levels with ENh-OC treatment (Fig. 9A). This demonstrated the potential of ENh-OC as an adjuvant in APAP-induced ALI recovery. Additionally, the blood biochemistry panel revealed that alkaline phosphatase (ALP) (Fig. 9B), alanine transaminase (ALT) (Fig. 9C), and triglycerides (Fig. 9D) were elevated in the APAP group. However, the levels in the APAP + ENh-OC were comparable to those in the NT group. Elevated ALT and ALP in blood serum are hallmarks of ALI,[40] while heightened triglyceride levels have also been linked with hepatic damage caused by APAP.[41] ENh-OC shows promise as a healing agent for APAP-induced ALI by modulating ALP, ALT, and triglyceride levels in blood serum. Moreover, the weight of the liver was significantly reduced for the mice treated with APAP. No significant difference was observed between the NT and APAP + ENh-OC groups (Fig. 9E). This could be attributed to the overall well-being of the liver and protection from APAP-induced damage by ENh-OC. As the ENh-OC was administered concurrently with APAP, this *in vivo* model does not allow definitive separation of effects on the initial injury phase from effects on the subsequent recovery phase. Thus, these results demonstrate

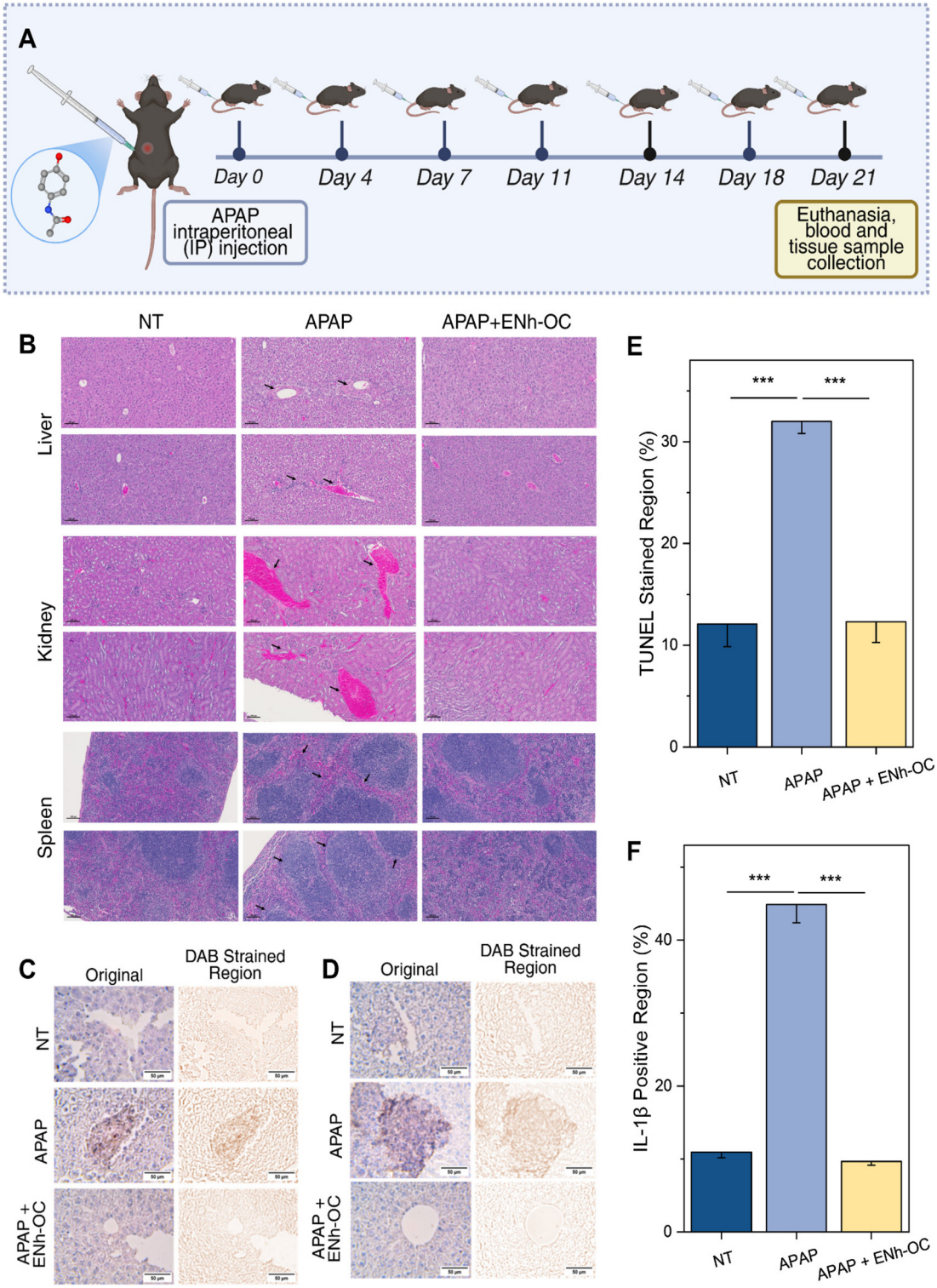

Fig. 8 (A) Timeline for 21-day efficacy study for ENh-OC mediated hepatic protection post-APAP intraperitoneal administration (Created in https://BioRender.com.), (B) H&E-stained liver, kidney, and spleen samples (scale bar = 100 μm), DAB-stained liver samples for (C) TUNEL assay, and (D) IL-1β (scale bar = 50 μm), (E) comparative TUNEL-stained region, and (F) comparative IL-1β-positive region. $n = 3$, $^{*}p \leq 0.05$, $^{**}p \leq 0.01$, and $^{***}p \leq 0.001$.

an overall protective effect rather than isolated promotion of post-injury recovery. Another limitation of this study is the 21-day endpoint, which does not necessarily capture acute injury resolution or early regenerative responses, a limitation in this study, studies with endpoints in the early stages should be done in the future. The long-term endpoint is selected to

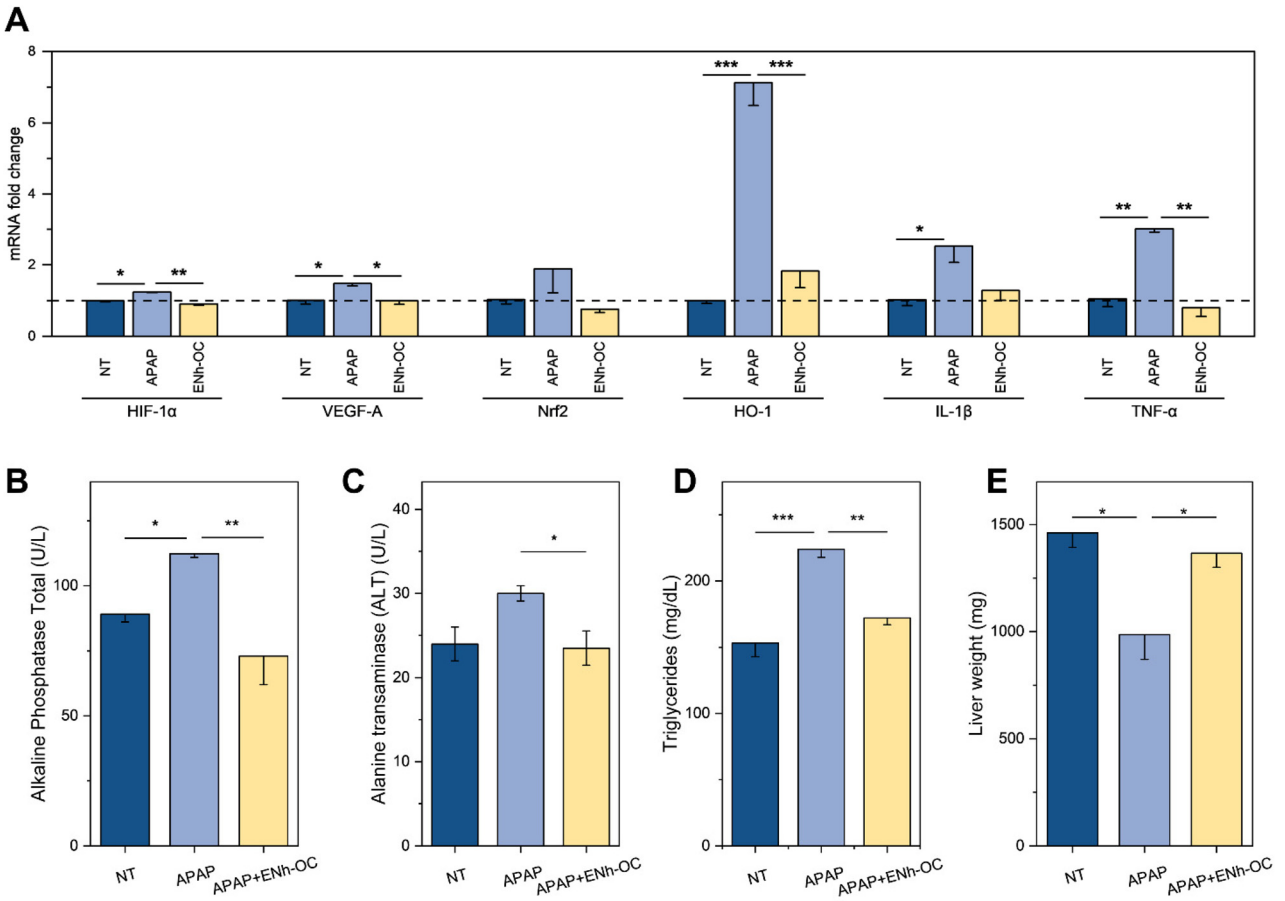

Fig. 9 (A) Modulation of hypoxia (HIF-1α, VEGF-A), oxidative stress (Nrf2, HO-1), and pro-inflammatory (IL-1β, TNF-α) genes with ENh-OC treatment post APAP administration, comparative levels of ALP (B), ALT (C), and triglycerides (D) in the blood serum, and comparative liver weights (E) among different treatment groups. $n = 3$, $*p \leq 0.05$, $**p \leq 0.01$, and $***p \leq 0.001$.

evaluate sustained tissue architecture protection at a delayed endpoint. Additionally, ENh-OCs have demonstrated effective recovery from APAP toxicity in a 72-hour spheroid model. However, further studies with a 48–96-hour endpoint will demonstrate injury resolution and early regenerative activity. ENh-OCs might have potential in mitigating the initial injury phase; these should be considered in the future. Experiments show that ENh-OC offers an overall long-term hepatic protection by mitigating hypoxia. It should be noted that hypoxia may not be prominent during the initial 0.5–2.0 hours of the injury phase.[7] Therefore, early-phase metabolic inhibition was not evaluated and is not proposed as a mechanism of action. However, as ENh-OC was co-administered with APAP, the possibility that the intervention influences the early injury phase cannot be excluded, and further experimental endpoint of 12–48 hours is essential for a more definitive mechanistic interpretation.

Overall, ENh-OC shows significant protection against APAP at the genetic, tissue, and blood serum levels. We hypothesize that synergistic anti-hypoxic, antioxidant, and anti-inflammatory functionalities offered by ENh-OC contribute to this protective effect and help maintain the native state in the liver tissue pre-APAP insult (Fig. 10). Hypoxia and HIF-1α signaling have been found to play a promoting role in APAP-induced hepatotoxicity.[6] We note that HIF-1α elevation under hypoxia causes upregulation of its target genes VEGF-A and HO-1.[42] Hypoxia upregulation of its target genes VEGF-A and HO-1.[42] Hypoxia also promotes the generation of ROS and superoxide, increasing the mitochondrial oxidative stress.[3] This in turn activates the Nrf2/HO-1 axis.[38] Additionally, HIF-1α also activates pro-inflammatory signaling and increases gene expression for pro-inflammatory cytokines such as IL-1β and TNF-α.[43] ENh-OC were able to inhibit HIF-1α signaling by controlled oxygen supply, and thus, were able to hinder the cascading reaction of oxidative stress and inflammation-related factors. Additionally, the anti-inflammatory and antioxidant components in blueberry exosomes, such as 5-hydroxymethyl furfural, campesterol, 4-vinylguaiacol, γ-tocopherol, *etc.*, were able to act as a secondary restraint for the downstream target genes such as VEGF-A, HO-1, IL-1β, and TNF-α. Necrotic hepatocytes release various damage-associated molecular patterns (DAMPs), which activate Kupffer cells to release pro-inflammatory cytokines such as IL-1β and TNF-α.[44] Kupffer cells then recruit neutrophils and M1 polarized macrophages, which rush to centrilobular hepatocytes, causing excessive immunoinfiltration to the damaged site.[3,45] We propose that ENh-OCs

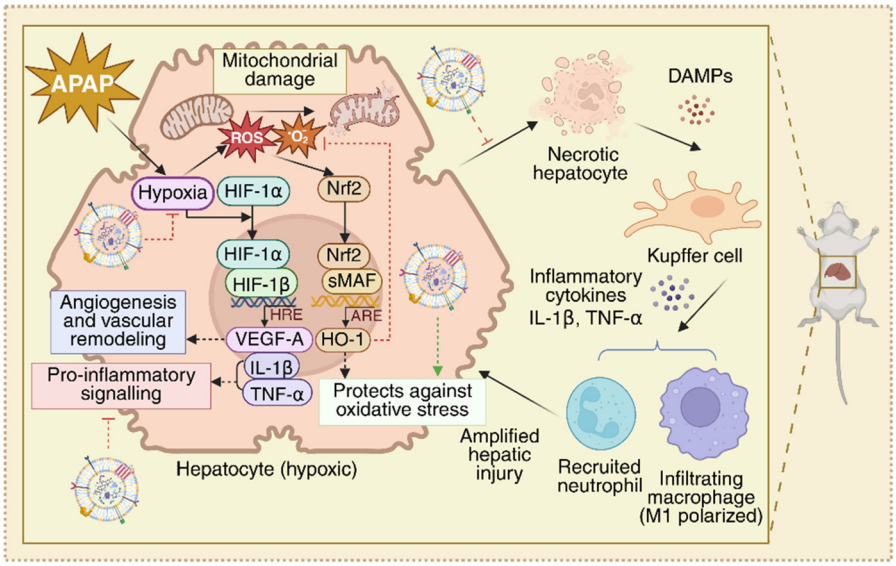

Fig. 10 Proposed mechanism of ENh-OC mediated protection from APAP-induced hepatic injury. ENh-OC downregulates the hypoxic gene HIF-1α and its downstream gene VEGF-A, thus helping to mitigate hypoxia by direct oxygen supply. This function of ENh-OC is verified by cell viability evaluation, where treated cells can withstand prolonged hypoxia without significant loss in viability. Moreover, ENh-OC combats oxidative stress by downregulating Nrf2 and HO-1. This effect is also evident in the inhibition of ROS and superoxide *in vitro* under hypoxic conditions. Additionally, ENh-OC downregulates pro-inflammatory genes IL-1β and TNF-α both *in vitro* and *in vivo*. Histology verifies this claim, as the ENh-OC-treated group shows less immune-infiltration than the APAP group. Overall, ENh-OC might have a protective effect against APAP-induced centrilobular necrosis, as observed from histology (Created in https://BioRender.com.).

were able to prevent centrilobular hepatic necrosis, as suggested by the histological tissue evaluation. Thus, it leads to limited inflammatory signaling and attenuated immuno-infiltration. Our study indicates that ENh-OC shows excellent promise for protection against APAP-induced ALI and positions it as a proof-of-concept platform technology against drug-induced acute liver injury.

Experimental methods

Materials

Pluronic® F-127 (P2443-250G), polysorbate 80 (59924-100 G-F), and fluorescent dye DiO (T40418-10MG) were purchased from Sigma-Aldrich®, USA. MCT oil, USP/NF (SKU C6003-80), was procured from SpecializedRx Products, LLC, USA. All chemicals were used as received without any modification.

Blueberry exosome extraction

Exosomes were extracted from blueberries following a previously reported protocol with necessary modifications.[46] Detailed steps of the procedure are depicted in SI Fig. 2. Briefly, 50 g of frozen fruits were washed with deionized water, mixed with 50 mL 1× PBS, and blended to obtain a slurry-like consistency. The blended liquid was then centrifuged at 2000*g* for 15 minutes, 8000*g* for 30 minutes, and 12 000*g* for 60 minutes at 4 °C, and palette was discarded in each step to remove large particles, dead cells, and cell debris, respectively (Eppendorf 5424R Refrigerated Centrifuge, Eppendorf AG, Germany). This was followed by ultracentrifugation of the supernatant at 200 000*g* for 120 minutes at 4 °C, collection of the pellet, and resuspension in cold (4 °C) 1× PBS to obtain 1 mg mL^{-1} exosome solution (Optima™ MAX-XP Ultracentrifuge, Beckman Coulter Inc., USA). The exosome solution was filtered using 0.22 μm syringe filters and stored at −80 °C until further use.

Exosome–niosome hybrid oxygen carrier (ENh-OC) synthesis

Pure oxygen at 10 psi was bubbled through water for injection (WFI) for 60 minutes to ensure complete saturation. Oxygen pressure increased to 20 psi, and oxygen purging was continued throughout the whole duration of the synthesis. The ENh-OC were synthesized utilizing pulse sonication mode with 40 seconds on and 30 seconds off cycles, and an amplitude of 40% (Branson SFX250 Sonifier w/Probe, Marshall Scientific, LLC., USA). Total synthesis time was 7 minutes, and 100 μL of 0.01 w/v% polysorbate 80, 0.01 w/v% Pluronic® F-127, 0.001 /v% MCT oil, and 0.1 w/v% exosomes were added to 9.6 mL of oxygen-saturated WFI at one-minute intervals. Freshly prepared ENh-OCs were filtered using a 0.22 μm syringe filter, transferred to glass vials, sealed with rubber stoppers, followed by aluminum caps, and stored at 4 °C. Additionally, niosome-oxygen carriers (N-OCs) were prepared following the same procedure as above, except without the addition of exosomes.

Fluorescent ENh-OC, N-OC, and exosomes (E) were prepared by incubating freshly prepared particles with 10 μM DiO (for *in vitro* testing) or DiD (for *in vivo* testing) solution (in DMSO solvent) for 60 minutes at room temperature, and

unbound dye was removed by lateral filtration using 100 kDa MWCO membrane filters by centrifuging at 1000*g* for 5 minutes (UFC810008, Amicon® Ultra, USA). For verifying the hybridization of E and N-OC to form ENh-OCs, E was labeled with DiO and N-OC with DiD, before ENh-OC synthesis. Spatial co-localization of DiO and DiD inside cells was utilized as an indirect way to assess the formation of ENh-OCs.

Optimization and characterization

ENh-OCs were optimized based on both sonication parameters (amplitude and on–off cycle duration) and concentration of the four components. At the first stage, a general full factorial model with two factors (amplitude and on–off cycle duration), and four levels (20, 30, 40, and 50% amplitudes, and on–off cycles of 40–30, 30–20, 20–10, and 10–5 seconds) was utilized. The optimal sonication parameters from this initial optimization was used in the second round of optimization, where a full factorial model with four factors (polysorbate 80, Pluronic® F-127, MCT oil, and exosomes concentration) and two levels (1×10^{-4}, and 1×10^{-5} w/v% for each of polysorbate 80, Pluronic® F-127, MCT oil, and 0.1 and 0.01 w/v% for exosomes) was utilized for optimizing the concentrations.

Exosomes were characterized with Gas Chromatography–Mass Spectrometry (GC-MS) (JMS-T2000GC AccuTOF™ GC-Alpha, JOEL Inc., USA). Exosome palette was solubilized in pure methanol to form a 10 mg mL^{-1} solution. GC-MS was performed with a high-resolution electron ionization (EI). The column has a length of 30 m, with an internal diameter of 0.2 μm, carrier gas velocity 0.02 cm s^{-1}, split ratio of 1 : 25. The cycle consisted of 1 minute hold at 80 °C, 80 to 150 °C with a ramp of 3 °C min^{-1}, 1 minute hold at 150 °C, 150 to 280 °C with a ramp of 20 °C min^{-1}, 26 minutes hold at 280 °C. The individual components were identified with the msFineAnalysis AI Software for AccuTOF GC (JOEL Inc., USA). Additionally, the protein and nucleic acid content in a 10 mg mL^{-1} exosome solution was quantified with NanoDrop™ One/OneC Microvolume UV-Vis Spectrophotometer (ND-ONE-W, Thermo Scientific™, USA).

The exosomes and optimized ENh-OC were characterized, where hydrodynamic diameter and zeta potential were measured with Litesizer™ 500 (Anton Paar USA Inc., USA), and particle concentration with Nanoparticle Tracking Analysis (NTA) (Nano-Sight NS300, Malvern Panalytical, USA) with a blue laser light source (λ = 488 nm). The samples were stained with uranyl acetate (2 w/v%), and TEM images were obtained by scanning transmission electron microscope (S)TEM (120 kV, 71 K magnification, AMT Camera Systems) (FEI Tecnai G2 F20 STWIN, Thermo Scientific™, USA).

Oxygen loading capacity, release, and storage

Oxygen holding and release capacity of the freshly prepared ENh-OCs were measured by Orion™ Versa Star Pro™ DO Benchtop Meter (VSTAR30, Thermo Scientific™, USA) following previously reported protocol.[47] To quantify the oxygen loading, the optical DO meter probe was placed in a glass tube and sealed with parafilm to create an enclosed system. The ENh-OCs were freshly prepared, diluted with deoxygenated water at a 25 : 75 ratio, and vacuumed for 30 minutes to remove oxygen that was not encapsulated within the nanocarriers. The dilution was performed as the total oxygen loaded in the ENh-OCs was higher than the measurable upper limit of the DO meter reading (20 mg L^{-1}). The diluted and vacuumed solution was then injected into the glass tube and further sealed with parafilm to create an airtight seal. The oxygen concentration was recorded at 1-minute intervals, and the oxygen holding capacity was calculated from the maximum recorded reading, where actual oxygen content = 4 × highest recorded DO meter reading in mg L^{-1}.

To assess oxygen release under physiological hypoxic conditions, an oxygen release profile was generated in a hypoxia chamber (continuously purged with nitrogen to maintain ~0.1v/v% O_2) at 37 °C. The ENh-OCs were diluted with deoxygenated water in a 5 : 5 ratio, and the DO was monitored at 1-minute intervals for 16 hours. Afterwards, the oxygen concentration *versus* time data was fitted into a biexponential kinetic model to quantify oxygen release rate. Additionally, to monitor the oxygen retention capacity, ENh-OCs were stored at 4 °C for up to 6 months. At one-month intervals, the retained oxygen was measured to verify long-term storage stability.

Evaluation of sterility

Soybean-casein digest media was prepared following the U.S. Pharmacopeia Sterility ⟨71⟩ recipe.[35] Briefly, casein peptone 1.7 w/v% (R451102, Remel Products, USA), 0.3 w/v% Peptone S (soy peptone) (30620061-1, BioWorld, USA), 0.5 w/v% NaCl (VW6430-1, VWR, USA), 0.25 w/v% K_2HPO_4 (7088-04, Mallinchrodt Chemicals, USA), and 0.23 w/v% dextrose (G7021-100G, Sigma, USA) were dissolved in 1 L of molecular biology grade water, pH was adjusted to 7.3 ± 0.2 using 1 M NaOH and autoclaved to ensure sterility. 9 mL of soybean-casein digest media was added to 1 mL of ENh-OC in sterile 15 mL tubes. Blank media was used as a negative control. For positive control, 15 mL tubes were directly inoculated with one of the following: *Bacillus subtilis*, *Escherichia coli*, *Pseudomonas aeruginosa 01*, and *Pseudomonas aeruginosa 14*. All samples were incubated at room temperature, and the optical density (OD600) was read daily for 14 days. OD600 reading was recorded daily for 500 μL of the sample with an Eppendorf BioPhotometer (6131, Marshall Scientific LLC, USA) against 1× PBS as a blank. Each group had three technical replicates.

Cell culture

LX-2 and HepG2 cells were cultured in a 5% CO_2 humidified incubator at 37 °C. The culture media for both cell lines consisted of DMEM (10-013-CV, Corning®, USA) supplemented with final concentrations of 1% antibiotic-antimycotic (100×) (15240096, Gibco™, USA), 1% Non-Essential Amino Acids Solution (100×) (11-140-050, Gibco™, USA), 2 mM L-glutamine (59202C-100ML, Sigma-Aldrich®, USA) and 10% fetal bovine serum (FBS) (A5670801, Gibco™, USA). TrypLE™ Express Enzyme (1×) (12605010, Gibco™, USA) was used for detaching

the cells. The cells used in this study were within passages 10–50.

Evaluation of protective effect against hypoxia

Cells were seeded in two 96-well black-walled plates at a density of 10 000 cells per well overnight to ensure attachment. The next day, cells were treated with ENh-OCs at different concentrations (5, 10, 25, and 50 v/v%) diluted with cell culture media and molecular biology-grade water (46-000-CM, Corning®, USA). The medium consisted of 50 v/v% of the media, and the remaining was adjusted with water. The no treatment (NT) group consisted of 50 v/v% of both medium and water. One plate was placed in a controlled gas chamber (3% O_2, 5% CO_2, and 92% N_2), and another group was subjected to normoxia, while both were incubated in a 37 °C incubator with 5% CO_2. MTT (3-(4,5-dimethylthiazol-2-yl)-2,5-diphenyltetrazolium bromide) (M6494, Invitrogen™, USA) assay was performed after 24 hours of either hypoxia or normoxia incubation to assess cell viability as per the manufacturer's protocol. Finally, absorbance was read at 570 nm using a microplate reader, and relative viability of the cells was calculated, taking the no-treatment (NT) group as a baseline. Each group had a total of eight technical replicates.

Evaluation of ROS and superoxide inhibition

ROS/Superoxide Detection Assay Kit (ab139476, Abcam Inc., USA) was used to determine the level of ROS and superoxide after treatment with exosomes (E), ENh-OC shell (ENh-S), and ENh-OC. Briefly, cells were cultured in a 96-well black-walled, clear-bottom plate overnight. The following day, the cells were incubated with E, ENh-S, and ENh-OC at a 25 v/v% concentration for 24 hours. On the third day, ROS/Superoxide detection was performed per manufacturer-instructed protocol, and fluorescence readings were then taken using a microplate reader to quantify ROS (Ex: 488 nm, Em: 520 nm) and superoxide (Ex: 550 nm, Em: 610 nm) generation. Each group had a total of four replicates.

Evaluation of uptake in cell monolayer

DiO-labeled E and DiD-labeled N-OCs were hybridized together to form ENh-OC. 200 000 cells were seeded in 35 mm glass-bottom Petri dishes overnight and treated with 25 (v/v%) ENh-OCs the following day for 6 hours. They were washed three times with 1× PBS to remove particles not taken up by the cells, fixed with 4% paraformaldehyde, stained with DAPI, and stored at 4 °C until imaging. Dark-field images were obtained by a Zeiss Axio Observer Z1 inverted research-grade microscope with 40× magnification (Carl Zeiss AG, USA). Co-localization of DiO and DiD labeled particles was used to verify hybridization and co-delivery of E and N-OCs in the form of ENh-OCs.

DiO-labeled E, N-OC, and ENh-OC were used to evaluate dose-dependent cell uptake. Cells were seeded at a density of 10 000 cells per well overnight. The following day, the old medium was discarded, and cells were incubated with fluorescent E, N-OC, and ENh-OC at different concentrations (5, 10, 25, and 50 v/v%), and incubated for 6 hours at 37 °C. The cells were then washed three times with 1× PBS to remove unbound particles, lysed with 1% Triton X-100 to release the endocytosed particles, and the fluorescent intensity was measured (Ex. 480 nm, Em. 525 nm) using a microplate reader. Each group had a total of eight replicates.

To visualize the cell uptake, cells were incubated with 25 (v/v%) DiO-labeled E, N-OC, E + N-OC, and ENh-OC for 6 hours, and cells were thoroughly washed with 1× PBS to remove the particles that were not internalized by the cells, fixed with 4% paraformaldehyde, and stained with DAPI (4′,6-diamidino-2-phenylindole) (D1306, Invitrogen™, USA). Finally, they were stored at 4 °C until imaging. Fluorescent images were obtained by a Zeiss Axio Observer Z1 inverted research-grade microscope with 10× magnification (Carl Zeiss AG, USA).

Evaluation of protection against APAP and uptake in spheroids

LX-2 spheroids were utilized to evaluate the protective effect of ENh-OC against APAP-induced toxicity. 5000 cells were seeded per well in 200 μL media in ultra-low attachment U-bottom plates (650901, Grainer, USA), centrifuged at 1000*g* for 5 minutes, and incubated overnight to form the spheroids (day 0). On day 1, the spheroids were treated with 5 mM APAP (except the NT group) or left untreated (for the NT group only). On day 2, they were treated with either E, ENh-S, or ENh-OC. On day 3, MTS reagent (3-(4,5-dimethylthiazol-2-yl)-5-(3-carboxymethoxyphenyl)-2-(4-sulfophenyl)-2*H*-tetrazolium) (ab223881, Abcam Inc., USA) was used to quantify (absorbance at 490 nm) and compare the viability of each group.

To assess the cell uptake in LX-2/HepG2 spheroids, spheroids were generated with 2500 cells of LX-2 and HepG2, following the previously delineated protocol. On the third day after spheroid initiation, they were incubated with either E, N-OC, or ENh-OC for 6 hours at 37 °C. Afterwards, the spheroids were washed three times with 1× PBS to remove unbound particles, fixed with 4% paraformaldehyde, stained with DAPI, and stored at 4 °C until imaging. Dark-field images were obtained by a Zeiss Axio Observer Z1 inverted research-grade microscope with 10× magnification (Carl Zeiss AG, USA).

Detection of gene expression modulation with RT-qPCR

Cells were seeded overnight in 6-well plates at a density of 300 000 cells per well. The following day, cells were treated with 25 v/v% of E, N-OC, and ENh-OC. Additionally, two no-treatment (NT) groups, one under normoxia (NT(nor)), and the other under hypoxia (NT(hyp)), were used as controls. The plates were transferred into the hypoxia chamber comprising 3% O_2, 5% CO_2, and 92% N_2 (except the NT(nor) group), and the chamber was placed in a 37 °C incubator for 24 hours. After a day, total RNA was extracted using the GeneJET RNA Purification Kit (K0731, Thermo Scientific™, USA), and cDNA was synthesized from RNA with the High-Capacity cDNA Reverse Transcription Kit (4368814, Applied Biosystems™, USA). Real-time qPCR was performed with StepOne™ Real-Time PCR System (4376357, Applied Biosystems™, USA) using PowerUp™ SYBR™ Green Master Mix for qPCR (A25742, Applied Biosystems™, USA). Expression levels of six key genes were assessed, among which two were related to hypoxia

(HIF-1α, VEGF-A), two were related to oxidative stress (Nrf2, HO-1), and the remaining two were related to inflammation (IL-1β, TNF-α). Finally, β-actin was used as the housekeeping gene to normalize relative gene expressions, and fold changes were calculated as $2^{-\Delta\Delta Ct}$. Primer sequences are provided in SI Table 1.

Assessment of *in vivo* safety, biodistribution, and efficacy

Experiments performed in this study were approved by the Institutional Animal Care and Use Committee under Protocol no. 24199: Treatment of ischemic diseases by oxygen nanoparticle therapy. An Association for Assessment and Accreditation of Laboratory Animal Care (AAALAC) International–accredited facility was used for housing the mice, provided with a 12-hour light/dark cycle, a standard chow diet, and an unlimited supply of clean drinking water. The animals were allowed to acclimate for 7 days before the procedure. For the safety study, 10 CD-1 female mice were used, divided into two groups with 5 mice in each. One group was injected with 300 μL ENh-OC (optimized formulation) through the tail vein (TV) on days 0, 3, 7, and 10, while the other received no treatment (NT) and was used as a control. Both groups were humanely euthanized on day 14, and tissue samples were collected, fixed with 10% formalin, and preserved for further analysis.

For the biodistribution study, 300 μL of DiD-conjugated optimized ENh-OC was administered to two NU/J mice *via* tail vein injection. The mice were scanned at 0, 2, 6, 24, 48, 72, and 96 hours following fluorescent ENh-OC administration with the PerkinElmer IVIS system in fluorescence mode (Ex. 633 nm, Em. 665 nm). At the end of 96 hours, the mice were euthanized, the collected organs (brain, heart, lung, stomach, spleen, liver, intestine, and kidney) were scanned, and the total radiant efficiency of each organ was quantified with Living Image® 4.5.2 Software.

For the efficacy study, 15 male C57BL/6 mice were used, divided into three groups, namely NT, APAP, and APAP + ENh-OC. The NT group did not receive any treatment and was used as a control. The APAP group received one intraperitoneal (IP) injection of 500 mg kg^{-1} APAP on day 0. The APAP + ENh-OC group received IP injection of APAP on day 0 and 300 μL TV injection of ENh-OC on days 0, 4, 7, 11, 14, 18, and 21. All mice were humanely euthanized on day 21, and blood and tissues were collected for future analysis.

For the safety study, representative liver, kidney, and lung tissue samples from NT and ENh-OC groups were stained with hematoxylin and eosin (H&E) and compared to assess any signs of toxicity. For the efficacy study, liver, kidney, and spleen samples were H&E-stained and compared based on tissue necrosis and immune-infiltration. RT-qPCR was used to quantify the expression levels of six genes of interest, namely, HIF-1α, VEGF-A, Nrf2, HO-1, IL-1β, and TNF-α in mouse liver tissues, with GAPDH as the housekeeping gene. Primer sequences are provided in SI Table 1. Additionally, blood biochemistry data were used to compare alkaline phosphatase (ALP), alanine transaminase (ALT), and triglycerides. Moreover, the TUNEL Assay was used to visualize DNA damage, and IL-1β immunofluorescent staining was used to assess inflammation in the liver tissue. 3,3′-Diaminobenzidine (DAB) staining was performed for both the TUNEL Assay and IL-1β staining, and ImageJ software was used to quantify the DAB-stained region.

Statistical analysis

Statistical analysis was performed using OriginPro (2024b) (OriginLab Corporation, USA). The differences between any two groups were analyzed using a two-tailed, unpaired Student's *t*-test. One-way ANOVA with Tukey's multiple comparisons was employed for comparisons involving more than two groups. Values of $p < 0.05$ were considered statistically significant. Moreover, *: $p < 0.05$, **: $p < 0.01$, ***: $p < 0.001$, ****: $p < 0.0001$ were used. The presented data indicate the mean ± SD from at least two independent experiments.

Conclusions

Acetaminophen (APAP)-induced acute liver injury (ALI) accounts for a huge portion of emergency hospital visits globally. Some trademark pathological traits of injured hepatic tissue are hypoxia, oxidative stress, and elevated pro-inflammatory signaling. Our current work comprises of an exosome–niosome hybrid oxygen carrier (ENh-OC) platform with hypoxia-mitigation, antioxidant, and anti-inflammatory properties to protect the liver from APAP-induced ALI. This nanoplatform is made from FDA-approved non-ionic surfactants such as polysorbate 80, Pluronic® F-127, medium chain triglyceride oil, and blueberry-derived exosomes, which have antioxidant and anti-inflammatory components. These sub-75 nm sized OCs offer sustained oxygen release for up to 16 hours, with a minimum shelf life of half a year. ENh-OCs have been found to combat cellular damage caused by prolonged hypoxia in LX-2 and HepG2 monolayers and showed a protective effect against APAP-induced cytotoxicity in LX-2spheroids for up to 24 hours. Moreover, ENh-OCs have been found to be safe for intravenous administration in a 14-day safety study, and their overall hepatoprotective effect has been demonstrated in a 3-week murine ALI model. RT-qPCR results verified the capability of ENh-OCs in modulating the expression of hypoxia (HIF-1α, VEGF-A), oxidative stress (Nrf2, HO-1), and pro-inflammatory (IL-1β, TNF-α) genes, indicating a potential role in addressing APAP-induced hepatic damage. We propose that the novel oxygen delivery platform conceptualized has the potential to safeguard hepatic tissue from APAP-induced acute liver damage by mitigating hypoxia, oxidative stress, and inflammation.

Author contributions

A. B. was responsible for the overall experimental design, formulation, experiments, results, and discussion, data analysis, first draft of the manuscript, and revisions; D. J. assisted with literature review, optimization, and *in vitro* studies;

T. L. assisted with *in vitro* and *in vivo* studies; X. H. assisted with *in vivo* studies and histological tissue processing; J. I. and A. B. conceived the idea; T. M. F. provided assistance and supervision in the *in vivo* studies and data analysis; G. H. U provided guidance and assisted with manuscript preparation; J. I. provided supervision and guidance on experimental planning and funding. All authors contributed to the writing of the manuscript and have read and approved the manuscript.

Conflicts of interest

J. I. and A. B. have applied for a patent (U.S. Patent Application No.: 63/844,253) based on the formulation utilized in this work. The remaining authors declare no conflict of interest.

Ethical statement

All animal procedures were performed in accordance with the Guidelines for Care and Use of Laboratory Animals approved by the Animal Ethics Committee of the University of Illinois, Urbana-Champaign. All studies conducted strictly adhered to Protocol no. 24199: treatment of ischemic diseases by oxygen nanoparticle therapy, approved by the Institutional Animal Care and Use Committee.

Data availability

All data supporting the findings of this study are available within the manuscript and the supplementary information (SI). Supplementary information: optimization, exosome extraction, and primer sequences. See DOI: https://doi.org/10.1039/d5bm01861g.

Additional raw data will be available from the corresponding author upon reasonable request.

Acknowledgements

Partial funding from the NSF STTR-Phase 2 grant (Award# 2236857) is acknowledged. Additionally, partial support from NIH 1R21EY035371-01 and the Carle-Illinois College of Medicine Seed grant is also acknowledged. We are thankful to the Tumor Engineering and Phenotyping (TEP) Shared Resources and the Comparative Biosciences Histology Laboratory for assistance in histological evaluation.

References

1 E. Yoon, A. Babar, M. Choudhary, M. Kutner and N. Pyrsopoulos, *J. Clin. Transl. Hepatol.*, 2016, **4**, 131–142.
2 Office of the Commissioner, Don't Overuse Acetaminophen,https://www.fda.gov/consumers/consumer-updates/dont-overuse-acetaminophen, (accessed September 18, 2025).
3 H. Jaeschke and A. Ramachandran, *Explor. Dig. Dis.*, 2025, **4**, 100569.
4 W. Bernal, G. Auzinger, A. Dhawan and J. Wendon, *Lancet*, 2010, **376**, 190–201.
5 E. S. Fisher and S. C. Curry, *Adv. Pharmacol.*, 2019, **85**, 263–272.
6 E. M. Sparkenbaugh, Y. Saini, K. K. Greenwood, J. J. LaPres, J. P. Luyendyk, B. L. Copple, J. F. Maddox, P. E. Ganey and R. A. Roth, *J. Pharmacol. Exp. Ther.*, 2011, **338**, 492–502.
7 S. Chaudhuri, S. S. McCullough, L. Hennings, L. Letzig, P. M. Simpson, J. A. Hinson and L. P. James, *Toxicol. Appl. Pharmacol.*, 2011, **252**, 211–220.
8 J. Cai, M. Hu, Z. Chen and Z. Ling, *J. Transl. Med.*, 2021, **19**, 186.
9 K. N. Huynh, S. Rao, B. Roth, T. Bryan, D. M. Fernando, F. Dayyani, D. Imagawa and N. Abi-Jaoudeh, *Cancers*, 2023, **15**, 2738.
10 S. D. Salhanick, B. Belikoff, D. Orlow, D. Holt, W. Reenstra and J. A. Buras, *Acad. Emerg. Med.*, 2006, **13**, 707–714.
11 M. Taslipinar, I. Aydin, U. Kaldirim, F. Aydin, M. Agilli, Y. Eyi, S. Tuncer, E. Altayli, F. Ucar, E. Macit, M. Toygar, N. Yigit and T. Cayci, *Hum. Exp. Toxicol.*, 2013, **32**, 1107–1116.
12 P. N. Bhandari, Y. Cui, B. D. Elzey, C. J. Goergen, C. M. Long and J. Irudayaraj, *Sci. Rep.*, 2017, **7**, 9268.
13 P. Bhandari, G. Novikova, C. J. Goergen and J. Irudayaraj, *Sci. Rep.*, 2018, **8**, 3112.
14 V. Messerschmidt, W. Ren, M. Tsipursky and J. Irudayaraj, *Transl. Vis. Sci. Technol.*, 2023, **12**, 16.
15 W. Ren, V. Messerschmidt, M. Tsipursky and J. Irudayaraj, *ACS Appl. Nano Mater.*, 2023, **6**, 13116–13126.
16 W. Ren, M. Sands, X. Han, M. Tsipursky and J. Irudayaraj, *ACS Omega*, 2024, **9**, 24095–24104.
17 X. Han, A. Bushra, W. Ren, R. Lu, D. Um, L. Ju, T. Jensen, S. Paul, M. Mahoney, M. Tsipursky, G. Cheng and J. Irudayaraj, *ACS Nano*, 2025, **19**, 41044–41061.
18 M. Peng, M. Shao, H. Dong, X. Han, M. Hao, Q. Yang, Q. Lyu, D. Tang, Z. Shen, K. Wang, H. Kuang and G. Cao, *Commun. Biol.*, 2023, **6**, 184.
19 T. Zhou, X. Liang, P. Wang, Y. Hu, Y. Qi, Y. Jin, Y. Du, C. Fang and J. Tian, *ACS Nano*, 2020, **14**, 12679–12696.
20 X. Han, C. Saengow, L. Ju, W. Ren, R. H. Ewoldt and J. Irudayaraj, *Nat. Commun.*, 2024, **15**, 3435.
21 X. Han, L. Ju, M. Sands, Y. Zhao and J. Irudayaraj, *ACS Pharmacol. Transl. Sci.*, 2025, **8**, 602–612.
22 A. Bushra, M. Fall, W. Ren, J. Igbalaye and J. Irudayaraj, *ACS Pharmacol. Transl. Sci.*, 2025, **8**, 2814–2829.
23 A. Moammeri, M. M. Chegeni, H. Sahrayi, R. Ghafelehbashi, F. Memarzadeh, A. Mansouri, I. Akbarzadeh, M. S. Abtahi, F. Hejabi and Q. Ren, *Mater. Today Bio*, 2023, **23**, 100837.
24 R. Kalluri and V. S. LeBleu, *Science*, 2020, **367**, 6977.
25 A. Sarasati, M. H. Syahruddin, A. Nuryanti, I. D. Ana, A. Barlian, C. H. Wijaya, D. Ratnadewi, T. D. K. Wungu and H. Takemori, *Biomedicines*, 2023, **11**, 1053.

26 E. Książek, Z. Goluch and M. Bochniak, *Nutrients*, 2024, **16**, 2940.
27 W. Zhao, Y. Bian, Q. Wang, F. Yin, L. Yin, Y. Zhang and J. Liu, *Acta Pharmacol. Sin.*, 2021, **43**, 645–658.
28 FDA/Center for Drug Evaluation and Research, Inactive Ingredient Search for Approved Drug Products, https://www.accessdata.fda.gov/scripts/cder/iig/index.cfm?event=BasicSearch.page, (accessed October 23, 2025).
29 K. A. Traul, A. Driedger, D. L. Ingle and D. Nakhasi, *Food Chem. Toxicol.*, 2000, **38**, 79–98.
30 W. Li, X.-N. Qu, Y. Han, S.-W. Zheng, J. Wang and Y.-P. Wang, *Int. J. Mol. Sci.*, 2015, **16**, 2446–2457.
31 Q. Ye, N. Georges and C. Selomulya, *Trends Food Sci. Technol.*, 2018, **78**, 167–179.
32 T. Esatbeyoglu, K. Ulbrich, C. Rehberg, S. Rohn and G. Rimbach, *Food Funct.*, 2015, **6**, 887–893.
33 B. Es-Sai, H. Wahnou, S. Benayad, S. Rabbaa, Y. Laaziouez, R. El Kebbaj, Y. Limami and R. E. Duval, *Molecules*, 2025, **30**, 653.
34 W. Schwab, *Molecules*, 2013, **18**, 6936–6951.
35 K. D. R. Ramarao, Z. Razali, C. Somasundram, W. Kunasekaran and T. L. Jin, *Molecules*, 2024, **29**, 1762.
36 Food and Drug Administration, Guidance for industry: Sterile Drug Products Produced by Aseptic Processing—Current Good Manufacturing, *Practice*, 2004 https://www.fda.gov/media/71026/download (accessed November 13, 2025).
37 S. Ramakrishnan, V. Anand and S. Roy, *J. Neuroimmune Pharmacol.*, 2014, **9**, 142–160.
38 T. Bae, S. P. Hallis and M.-K. Kwak, *Exp. Mol. Med.*, 2024, **56**, 501–514.
39 H. K. Eltzschig and P. Carmeliet, *N. Engl. J. Med.*, 2011, **364**, 656–665.
40 X. Li, J. Ni and L. Chen, *Front. Pharmacol.*, 2023, **14**, 1239395.
41 H. S. Buttar, E. A. Nera and R. H. Downie, *Toxicology*, 1976, **6**, 9–20.
42 Q. Chu, X. Gu, Q. Zheng and H. Zhu, *Ann. Transl. Med.*, 2022, **10**, 109.
43 X. Kong, W. Liu, X. Zhang, C. Zhou, X. Sun, L. Cheng, J. Lin, Z. Xie and J. Li, *FASEB J.*, 2023, **37**, 23140.
44 O. Krenkel, J. C. Mossanen and F. Tacke, *Hepatobiliary Surg. Nutr.*, 2014, **3**, 33143–33343.
45 T. Yang, H. Wang, X. Wang, J. Li and L. Jiang, *Biology*, 2022, **11**, 1057.
46 Y. Leng, L. Yang, S. Pan, L. Zhan and F. Yuan, *Food Sci. Hum. Wellness*, 2024, **13**, 869–878.
47 A. Bushra, W. Ren, D. Um, X. Han, M. Tsipursky and J. Irudayaraj, *Biomater. Sci.*, 2025, **13**, 6098–6112.